Connective Tissue Research

ISSN: (Print) (Online) Journal homepage: https://www.tandfonline.com/loi/icts20

Spatial frequency metrics for analysis of microscopic images of musculoskeletal tissues

Kayvan Forouhesh Tehrani, Emily G. Pendleton, W. Michael Southern, Jarrod A. Call & Luke J. Mortensen

To cite this article: Kayvan Forouhesh Tehrani, Emily G. Pendleton, W. Michael Southern, Jarrod A. Call & Luke J. Mortensen (2021) Spatial frequency metrics for analysis of microscopic images of musculoskeletal tissues, Connective Tissue Research, 62:1, 4-14, DOI: 10.1080/03008207.2020.1828381

To link to this article: https://doi.org/10.1080/03008207.2020.1828381

CONNECTIVE TISSUE RESEARCH
2021, VOL. 62, NO. 1, 4–14
https://doi.org/10.1080/03008207.2020.1828381

Taylor & Francis
Taylor & Francis Group

Spatial frequency metrics for analysis of microscopic images of musculoskeletal tissues

Kayvan Forouhesh Tehrani [a], Emily G. Pendleton [a], W. Michael Southern [b,c], Jarrod A. Call [a,b], and Luke J. Mortensen [a,d]

[a]Regenerative Bioscience Center, Rhodes Center for ADS, University of Georgia, Athens, GA, USA; [b]Department of Kinesiology, University of Georgia, Athens, GA, USA; [c]Currently with Department of Biochemistry, Molecular Biology, and Biophysics, University of Minnesota, Minneapolis, MN, USA; [d]School of Chemical, Materials and Biomedical Engineering, University of Georgia, Athens, GA, USA

ABSTRACT

Purpose: Imaging-based metrics for analysis of biological tissues are powerful tools that can extract information such as shape, size, periodicity, and many other features to assess the requested qualities of a tissue. Muscular and osseous tissues consist of periodic structures that are directly related to their function, and so analysis of these patterns likely reflects tissue health and regeneration.

Methods: A method for assessment of periodic structures is by analyzing them in the spatial frequency domain using the Fourier transform. In this paper, we present two filters which we developed in the spatial frequency domain for the purpose of analyzing musculoskeletal structures. These filters provide information about 1) the angular orientation of the tissues and 2) their periodicity. We explore periodic structural patterns in the mitochondrial network of skeletal muscles that are reflective of muscle metabolism and myogenesis; and patterns of collagen fibers in the bone that are reflective of the organization and health of bone extracellular matrix.

Results: We present an analysis of mouse skeletal muscle in healthy and injured muscles. We used a transgenic mouse that ubiquitously expresses fluorescent protein in their mitochondria and performed 2-photon microscopy to image the structures. To acquire the collagen structure of the bone we used non-linear SHG microscopy of mouse flat bone. We analyze and compare juvenile versus adult mice, which have different structural patterns.

Conclusions: Our results indicate that these metrics can quantify musculoskeletal tissues during development and regeneration.

ARTICLE HISTORY
Received 22 May 2020
Accepted 22 September 2020

KEYWORDS
Musculoskeletal tissues; Fourier metric; multiphoton microscopy

1. Introduction

Musculoskeletal tissues, whose function is contingent on their physical and mechanical properties, often have well-defined periodic structural elements in their normal healthy state. In skeletal muscle and bone, these periodic structures appear at the microscale and are assembled to provide critical functional properties in the macroscopic tissue. During maturation, injury, and regenerative processes, tissue structure is strongly altered, and therefore techniques that enable evaluation of periodicity are critical for understanding musculoskeletal health and structural properties.

In the skeletal muscle, muscle fibers are composed of several dimensions of structural periodicity ranging from the myofibril to the muscle fiber to the fascicle that generates and propagates contractile force relying on effective energy transfer through a well-organized network of mitochondria[1-3]. Bone, the most structurally rigid tissue in the body, is another example of a periodic layered construct, in which collagen fibers are grouped together to make lamellar sheets[4]. Each sheet is made of fibers that are aligned in a coordinated fashion, with multiple sheets stacked at rotated orientations to form a 3-dimensional mesh, which provides the overall mineralized bone tissue with ductility and toughness[5,6]. These structural features of muscles and bones are implicit, if not inherent, to their physiology. Theoretically, the definition of temporal responses to these structures, such as occurring with injury or disease, can be leveraged to make inferences regarding i) pathophysiology, ii) identification of targets for regeneration, and iii) validation of restorative approaches.

Longitudinal image-based analysis strategies are ideal for the investigation of temporal responses of muscle and bone periodic structures, with the

CONTACT Luke J. Mortensen luke.mortensen@uga.edu Regenerative Bioscience Center, Rhodes Center for ADS and School for Chemical, Materials and Biomedical Engineering, University of Georgia, Athens, GA 30602, USA
Supplemental data for this article can be accessed here.

possibility of multiple imaging sessions over a period of weeks or months[7]. However, some image-based methods for the analysis of tissue structure often emphasize spatial domain features such as morphology, contours, geometry, feature extraction, wavelet analysis, and machine learning methods[8-11]. These methods can be computationally intensive, time-consuming, and often perform poorly in low signal-to-noise ratio environments. They also are susceptible to fluctuations in noise and signal intensity across an image, and typically require retuning even with small variations in noise or object intensity such as can occur between imaging sessions. Fourier Transform (FT) analysis is an alternate approach that describes an image by its periodicity and related properties (e.g., angle and phase). Therefore, this method is very fruitful for analyzing structures that have periodic features while reducing sensitivity to noise and algorithmic complexity.

Fourier-based analysis has found broad application for analyzing the health, development, and regeneration of periodic structures common in biology[12-17] such as autofluorescence imaging of mitochondrial organization[18-21], morphological evaluation of spermatozoa ellipticity[22], second harmonic generation (SHG) imaging of actin and myosin banding regularity in muscle[23] SHG imaging of orientation and organization of collagen in epithelial tissues[24,25], and SHG imaging of musculoskeletal tissues[26-28]. These analyses frequently involve direct quantification of the FT[22,24,25] or its magnitude squared form, known as the power spectrum[14-17,29–33]. Spectral moment invariants (SMI) of the power spectrum[29] have been used for analysis of scale and rotation invariant images, including SHG image analysis[30-33]. This method gives different weights to different frequency components of the power spectrum, which enables quantification of images with multiple feature types.

In this work, we present two Fourier-based metrics for analysis of the structural organization of musculoskeletal structures by the volumetric assessment of angular integrity and periodicity consistency. These metrics use FT to convert an image from the spatial domain into its frequency components, which represent the structures' periodicity and angle depending on their location within the frequency domain. The first metric presented here is an angular Fourier filter (AFF), which analyzes the orientation of a structure regardless of its frequency. Because muscle and bone have very directionally organized structures in their healthy state, this metric can assess the state of the tissue in the course of a regeneration process or a diseased state. The second metric is a radial Fourier filter (RFF), which describes an image based on the period of the features within a structure (frequency). For instance, since healthy muscles have a known striation period, an image of this pattern using fluorescence of the mitochondrial network or SHG signal from actin/myosin bands will produce a strong peak at a characteristic frequency. However, if the muscle is damaged or the periodicity is reduced, the dominance of the characteristic peak would diminish. These metrics are different from SMI analysis in that AFF and RFF are designed explicitly to give a score based on rotation and periodicity of the image features and not an overall score for the whole image. In this paper, we first present AFF and its application in the analysis of healthy skeletal muscle using fluorescent 2-photon excitation fluorescence imaging of mitochondria and label-free SHG imaging of actin/myosin bands, and then to evaluate injury severity and regeneration after volumetric muscle loss (VML) injury. We also applied this method for polarimetric assessment of collagen fibers within lamellae sheets of the bone using label-free second harmonic generation (SHG) microscopy. We then investigate the use of our RFF metric for analysis of muscle response to a VML injury at different stages of the regeneration process. Our results suggest that these metrics can provide meaningful evaluation of tissue organization and repair.

2. Materials and methods

2.1. Multiphoton microscope

We used a home-built multiphoton microscope with a Ti:Sapphire laser (Coherent Chameleon Ultra II), a 60x water immersion objective lens with NA of 1.1 (Olympus LUMFLN 60x), a resonant-galvanometer scan system (Sutter instruments MDR-R), two photon multiplier tubes (Hamamatsu H10770-40) and transimpedance amplifiers (Edmund Optics 59–178), and a FPGA (National Instruments) digitizer for signal collection. A 509/22 nm (Semrock) filter was used for 2-photon excitation imaging of GFP (Dendra2) with 836 nm excitation light (130 fs). SHG imaging was performed using a 390/18 nm (Semrock) filter with 775 nm excitation. A broadband linear polarizer (Edmund Optics 49–229) mounted on a motorized rotational stage was placed before the scan system for polarimetry. In non-polarimetric SHG imaging experiments, the angle of the polarizer was adjusted to maximize the output signal. More details can be found in reference[34].

2.2. Muscle injury and sample preparation

Muscle samples were extracted 1 hour before imaging from a transgenic mouse with C57Bl/6 background, which ubiquitously expresses mitochondrial Dendra2 green/red photoswitchable monomeric fluorescent protein (Jackson Laboratory, #018385)[35]. Volumetric muscle loss (VML) injury was conducted on the hindlimbs of anesthetized (isoflurane 1.5–2.0%) mice, as previously described[36]. All mice received administration of buprenorphine-SR (1.2 mg/kg; s.c.) for pain management 30 minutes prior to surgery. An anterior incision was made to expose the tibialis anterior (TA) muscle and the fascia was removed. A 3-mm biopsy punch was used to surgically create the VML injury in the middle of the muscle (7.46 ± 1.2 mg removed). Following the VML injury, the skin incision was sutured closed (6–0 silk). We have previously reported that this VML injury causes an immediate and lasting decrement in muscle contractile and metabolic function[36,37]. However, mice remain mobile in the cage and there are no observed changes in food or water consumption. The mice were observed daily and were excluded if there was a significant loss of body mass (10%) in the first days post-surgery or if continued lethargy and lameness is noted. Otherwise there were no adverse events noted related to the VML surgery. Animals were randomized into VML or sham surgery. The investigators conducting the experiments were aware of the group allocations, and no blinding procedure was performed. Confounders that were controlled were housing, temp, light/dark cycle, body mass, lameness, lethargy as already stated. No other confounders were controlled for. Supplemental Figure 1 shows the procedures followed for VML injury generation.

All the muscle-related animal procedures were designed prior to the experiment, and performed in accordance with the University of Georgia Institutional Animal Care and Use Committee (IACUC) under protocol number A2017 08–004-Y3-A3. More information on animal housing can be found in the supplemental information.

2.3. Bone sample preparation

Skull samples were collected from wild type B6/129 mice in this study. Juvenile and adult mice were sacrificed at two and twelve weeks of age, respectively. The skulls were then skinned and embedded in silicone to prevent movement. Skulls were stored in 70% ethanol at room temperature. For imaging, the skulls were immersed in phosphate buffered saline (PBS). 3D polarimetric SHG images were acquired from the skull in the area on the sides of the sagittal suture and posterior of the coronal suture. Supplemental Figure 2 shows the procedures followed for imaging of skull *in vivo*. Imaging and osseous experiments were designed prior to the experiment, and performed under IACUC protocol number A2018 06–008-Y3-A11.

2.4. Angular Fourier Filtering

In the Fourier domain, signals (spatial or temporal) are described in terms of a complete set of sine and cosine functions. Therefore, larger features that make up the low-frequency components are represented in the areas closer to the center, and the finer features that produce high-frequency components are farther from the center. At the center, the zero-frequency or DC component of an image, (the average of the whole image) is located. It should be noted that sharp edges of large features are also made of high-frequency components (Figure 1 (a-d)). In an optical microscope, the diffraction-limited resolution is a function of the wavelength of light and the numerical aperture of the microscope[38], which defines the finest structure or the highest frequency that can be captured. In the FT, this can be represented by a circle whose diameter reflects the maximum frequency of the fluorescent microscope. An intrinsic property of the FT is that it retains angular information about the sample, therefore if the image features are rotated the frequency components are also rotated respectively (Figure 1(e-h)). To evaluate the directionality of the tissue structures, we exploit this property and apply an angular Gaussian filter normalized by all the frequency components to extract AFF information.

Angular information extraction, therefore, requires a wedge-shaped filter (ψ) with a Gaussian profile w.r.t. φ in cylindrical coordinates ρ,φ, (Figure 1(i)). The filter is defined using:

$$\Psi_{AFF}(\rho,\varphi,\alpha) = \exp\left(\frac{-(\varphi-\alpha)^2}{2\sigma^2}\right), \qquad (1)$$

where α is the angle of the filter, and σ is the filter's e^{-2} bandwidth. The next step in this analysis is to calculate the 2D Fourier transform of the image and apply the filter at rotation angles 0-π. Since in this paper, we use image stack of both volume and polarization, we generalize the equation to state f (depth z, or polarization p). The FT of each image i within a stack in cylindrical coordinates:

$$I(\rho,\varphi,f) = \mathcal{F}\{i(\bar{r})\}(f) \rightarrow r^2 = x^2 + y^2. \qquad (2)$$

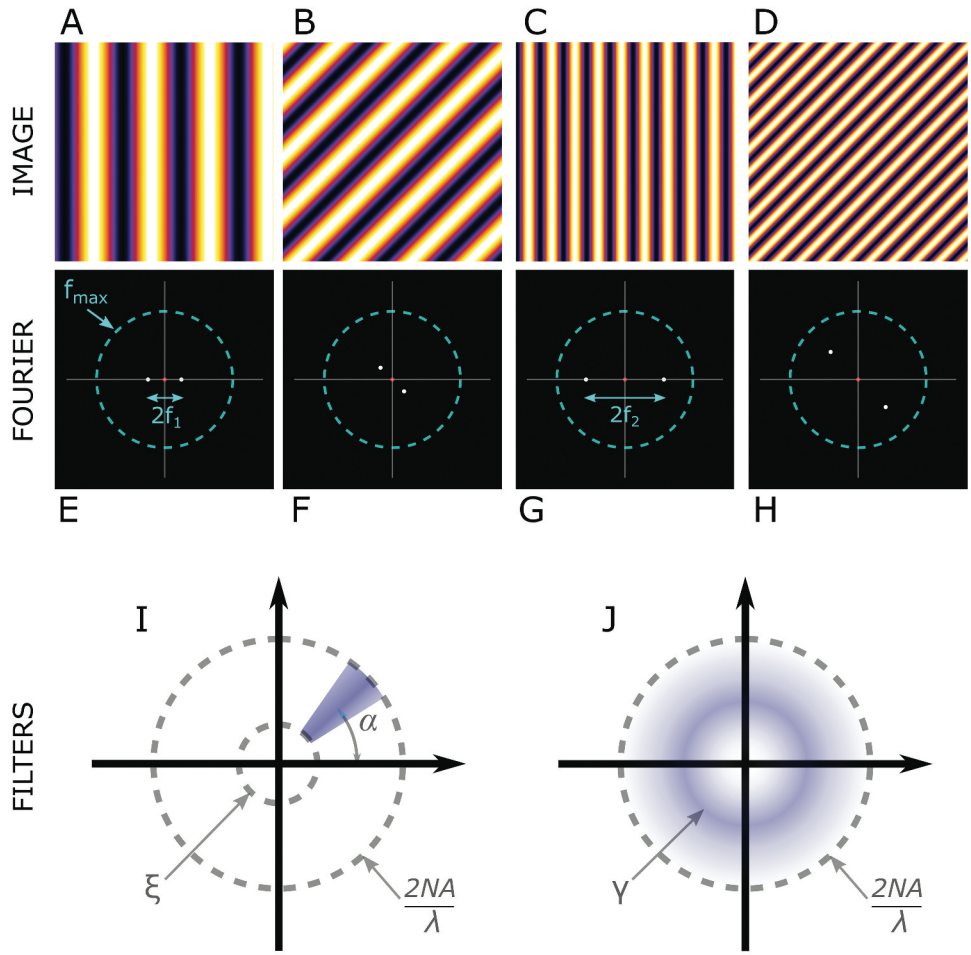

Figure 1. Representation of the image content, its frequency contents, and the Fourier metrics for image analyses. (a-b) show images of a low-frequency (larger features) pattern at 0° and 45°. Their corresponding frequency contents are shown in E and F, respectively. fmax is the maximum frequency content that the imaging system can acquire. Similarly, images of a high-frequency pattern (smaller features) are shown in (c-d), and their frequency domain information in (g and h). In the Fourier domain, the zero frequency or the DC component is shown as a red dot. The Fourier filters are shown in (i and j). (i) is the representation of the angular Fourier filter, which has a Gaussian profile with regard to the angle. (j) shows the high-frequency content filter with Gaussian profile with regard to the radius.

where $\mathcal{F}$is the FT operator and the line on r shows its vectorial nature. Due to the symmetrical nature of the Fourier transform, evaluating angles from 0 to π will provide us with information about all the frequency components. By rotating the Gaussian wedge filter at a given depth or polarization state, the AFF metric produces a 2D histogram that is calculated using:
where M is a circular mask defined by the resolution-limit of the imaging system. The outer diameter of M is determined by the maximum resolution of the imaging system (numerical aperture of the microscope *NA* and the wavelength of the emitted light λ) to limit high-frequency noise, its inner diameter is defined by a low-frequency cutoff ξ frequency:

$$M(\rho,\varphi) = \begin{cases} 1 & \xi < \rho < (2NA/\lambda) \\ 0 & otherwise. \end{cases} \quad (4)$$

The low-frequency bound of the filter, limits contribution of the larger features that do not necessarily contain useful information about the structures under study, and yields a frequency pass-band that can be precisely tuned to study structures of a biologically relevant size range.

Finally, for further quantification of the whole structure, we calculate an alignment ratio (AR). AR determines the directionality of the entire stack of images by calculating the concentration of frequency components (maximum of AFF in state *f*) normalized by all frequency components:
where max and avg are the maximum and average operators, N is the number of images in the stack, and the symbol ∈ indicates set membership. An

organized network produces distinct AFF peaks, with a commensurate high AR value.

2.5. Radial Fourier Filtering

The RFF metric converts images from the spatial domain i to the Fourier domain I and filters the frequency contents to find the ratio of the contents of interest to all the frequency contents, *RFF*. It uses a ring-shaped bandpass filter with a Gaussian profile Ψ_{RFF} as a function of radius (Figure 1(j)), and e^{-2} bandwidth σ (in radial coordinates ρ,ϕ). The filter is described using

$$\Psi_{RFF}(\rho,\varphi,\gamma) = \exp\left(\frac{-(\rho-\gamma)^2}{2\sigma^2}\right). \quad (6)$$

Similar to equation 3, each point on the RFF 2D histogram is calculated by

$$RFF(\gamma,z) = \left(\frac{\sum_{\rho,\varphi}\left(|I(\rho,\varphi,z)| \times \Psi_{RFF}(\rho,\varphi,\gamma)\right)^2}{\sum_{\rho,\varphi}\left(|I(\rho,\varphi,z)|\right)^2}\right)^{1/2}. \quad (7)$$

This filter is inherently a Gaussian bandpass filter and therefore does not require the application of mask (Equation 5), however the maximum radius of the filter for calculation of RFF 2D histogram is defined by the resolution-limit. This metric is applied to 3D stacks for analysis of all angles of the frequency components over depth, and therefore the depth is indicated by z in this equation.

3. Results and discussion

3.1. AFF for muscle injury assessment

First, we applied the AFF metric to image stacks acquired in the soleus muscle of a healthy transgenic mouse expressing green fluorescent protein (GFP)[37] in its mitochondria (Figure 2(a)). Both the mitochondrial network and the actin/myosin bands were imaged simultaneously for structural analysis, in GFP and SHG channels respectively. Since soleus is a slow-twitch muscle, its mitochondrial network is highly organized in two distinct directions (Figure 2(b)). AFF analysis of the muscle clearly identifies these structures. SHG imaging of the muscle was performed with laser polarization optimized for a single direction of the structure (actin/myosin), and therefore a single peak with strong amplitude can be observed (Figure 2(c)). We empirically found that SHG imaging within the muscle requires careful removal of fascia and other connective tissues. That is most likely due to the optically distorting nature of the fascia and relatively low backscattering of the forward-generated SHG from underlying layers of muscle (in comparison to mineralized bone). Therefore, its maximum achievable imaging depth is limited compared to 2-photon excitation imaging of GFP tagged mitochondria.

Second, we applied AFF for the analysis of muscle recovering from VML injury. For this purpose, we used the TA muscle of our mito-GFP transgenic mouse model. We acquired 3D stacks of images of 1) intact skeletal muscle, 2) immediately post-VML muscle, and 3) 7-day post-VML muscle (Figure 3). The AFF is well suited to detect the presence of the intact mitochondrial network that is a periodic structure containing two dominant angles in the healthy muscle (Figure 3(a)). The Fourier transform (Figure 3(d)) shows strong peaks at the tissue's characteristic frequency component. The mitochondrial network is organized parallel to the muscle fiber orientation as well as in orthogonal bands perpendicular to the muscle fibers. These two dominant peaks can be seen when examining a heatmap of the AFF as a function of depth (Figure 3(g)). Immediately after VML damage, the impaired organization of the muscle is reflected in its reduced spatial domain spectrum support (Figure 3(b,e,h)). Mitochondrial organization disruption continues out to 7 days after injury, as evidenced by further reduction in the organized spatial domain (Figure 3(c,f,i)). The loss of organization is also represented by the respective AR values of these 3 different states (Figure 3(j)), and clearly indicate the loss of organization from injury and the tissue injury response.

3.2. Application of AFF for bone collagen polarimetry analysis

Next, we applied AFF to SHG polarimetric analysis of bone collagen fiber organization. Fibrillar type 1 collagen fibers produce SHG signal when exposed to high energy femtosecond pulses, with the emitted intensity proportional to the alignment of the fiber orientation and the incident light polarization[39,40]. Bone structure is under constant remodeling, with the collagen fibrous mesh and mineral deposits cyclically reclaimed by osteoclasts, while new collagen mesh and mineral are produced at osteogenic sites by osteoblasts. This bone deposition/resorption process occurs rapidly in the juvenile bone to accommodate growth. During this time of active development and growth, the bone has not achieved full lamellar organization, and the collagen mesh structure is in a looser and less-organized state commonly known as

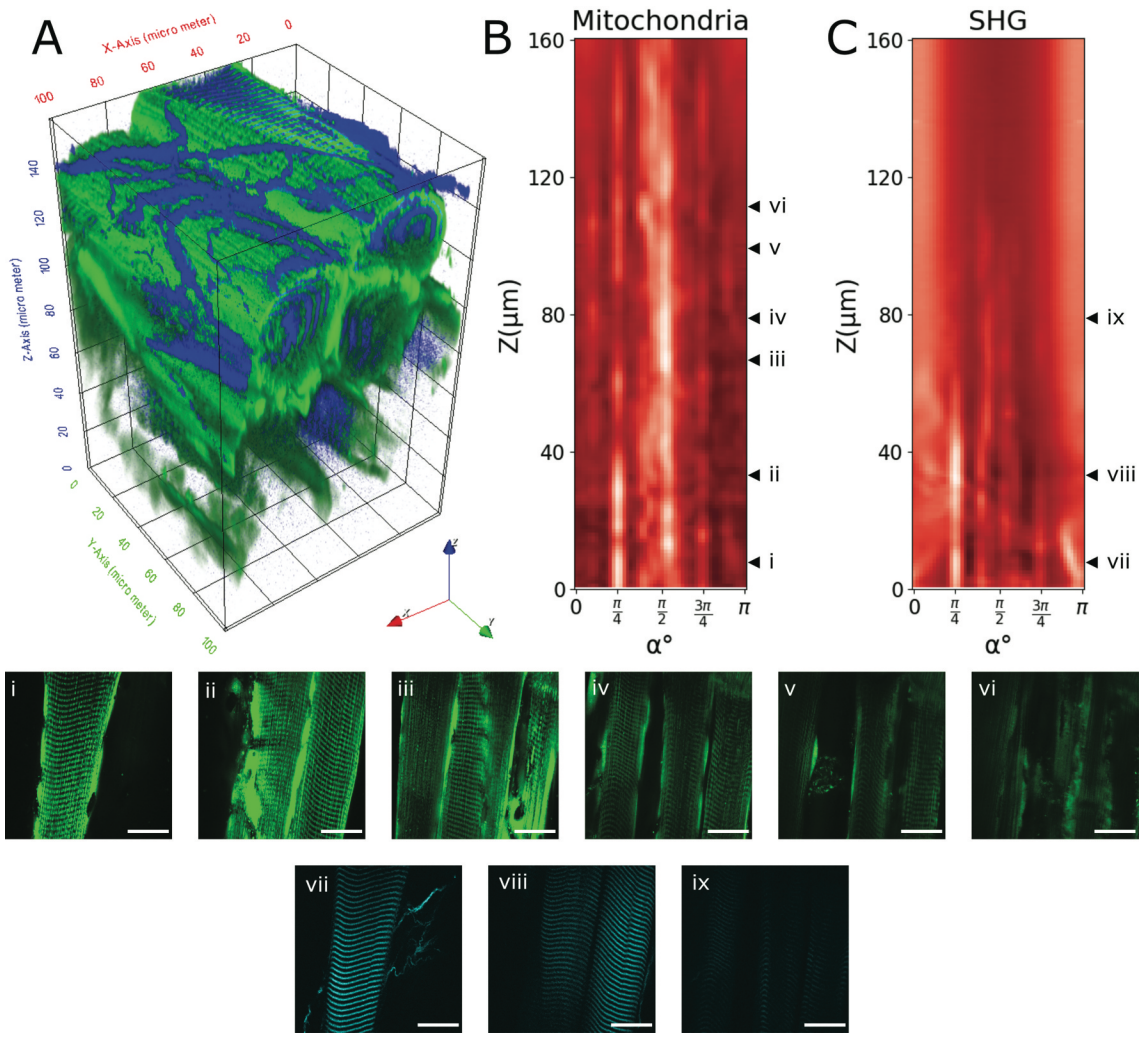

Figure 2. Angular Fourier Filter for analysis of a healthy soleus muscle mitochondrial network and collagenous structure (SHG). A 3D view of the soleus muscle mitochondria and SHG imaging is shown in (a), with AFF analysis of mitochondrial fluorescence (b) and SHG bands (c). Cross-sections of mitochondria and SHG at different depths are shown in (i–ix). Since SHG imaging is more sensitive to optical distortions, the maximum achievable depth is more limited compared to two-photon GFP imaging of mitochondria. Scale bars are 25 µm.

woven bone. The collagen mesh of juvenile bone (Figure 4(a)) is not as compact and organized as adult collagen (Figure 4(b)). Thus, the resulting polarimetry of the less compact juvenile bone shows polarized light at different orientations, suggesting that the collagen fibers in a plane are less well organized, with a potential contribution from the backscattered light produced by out of plane collagen fibers. Mature adult bone has a dense collagen mesh and well-defined collagen fibers are observed with similar orientations in regions across the field of view. Although the Fourier transform of juvenile bone (Figure 4(c,c')) does reflect the organization of the fibers, the Fourier transform of the adult bone image (Figure 4(d,d')) shows more definite directionality. Hence the AFF histograms in bone (Figure 4(e,f)) amplify this effect and show strong peaks at the corresponding angles with a sinusoidal trend with regard to the polarization.

3.3. Application of RFF for muscle healing evaluation

RFF analyzes structures' periodicity without taking their directionality into account. Therefore, it can visualize the total frequency content of a given structure. Muscle fiber structures are made of striations of a known frequency range that varies during contraction and relaxation. After a VML injury is made, the striation is disturbed and mostly replaced with layers of disorganized cells.

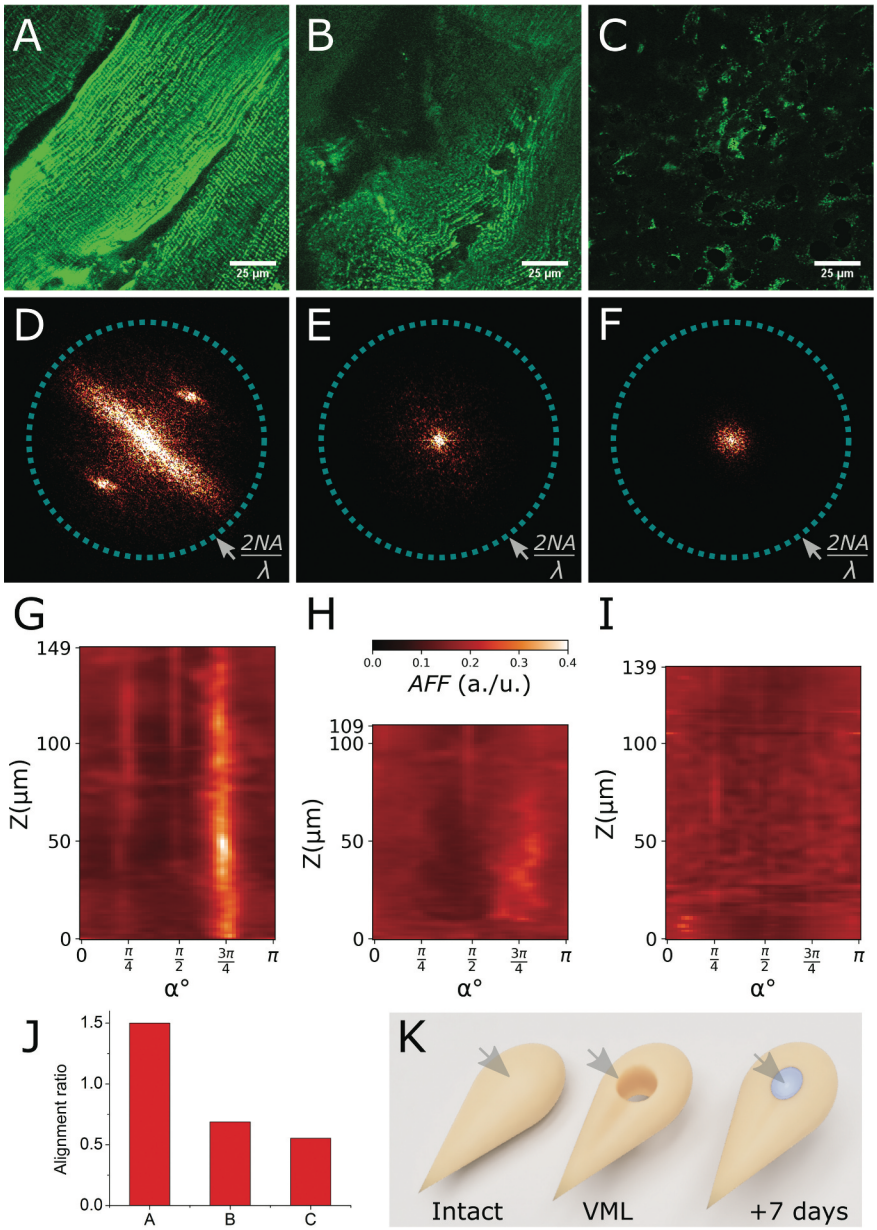

Figure 3. Angular Fourier Filter (AFF) for analysis on fluorescent 2-photon images of TA muscle mitochondrial network. An intact mitochondrial network is shown in (a). (b) and (c) panels show muscles immediately after a VML injury, and 7 days post-injury, respectively. The Fourier transform of the images in (a-c) are shown in (d-f), and their corresponding AFF analyses are shown in (g-i). The AFF analysis shows that the muscle with an intact mitochondrial network produces strong peaks, maintained over the depth of the volume, which suggests the strong organization of the structure. Immediately after the injury, the muscle has a jagged shape, which produces angularly scattered peaks over the depth. 7 days post-injury, numerous inflammatory cells have infiltrated the volume and few fibers are observed; therefore the AFF analysis does not produce any significant peak. The alignment ratio of these 3 conditions is shown in (j). (k) shows the location of imaging in intact, immediately after VML injury, and 7 days post-injury.

We applied the RFF metric to intact muscle fibers (Figure 5(a,d,g)), then to assess muscle healing after VML injury, we imaged 7 days post-injury (Figure 5 (b,e,h)) and 30 days post-VML injury (Figure 5(c,f,i)). The RFF histogram clearly shows a peak that is ongoing through the depth for the intact muscle (Figure 5(g)), which is also observed in the spatial domain morphology (Figure 5(a,d)). The 7-day post-injury case, however, does not show a significant frequency peak (Figure 5(h)), due to the presence of numerous disorganized cells in the injury site (Figure 5(b,e)). This is likely due to the extensive infiltration of inflammatory cells that occurs during the early stages of a VML injury. In the case of 30 days post-injury, the inflammatory cells were not detected (Figure 5(c,f)), and there appeared to be a reemergence of a muscle fiber

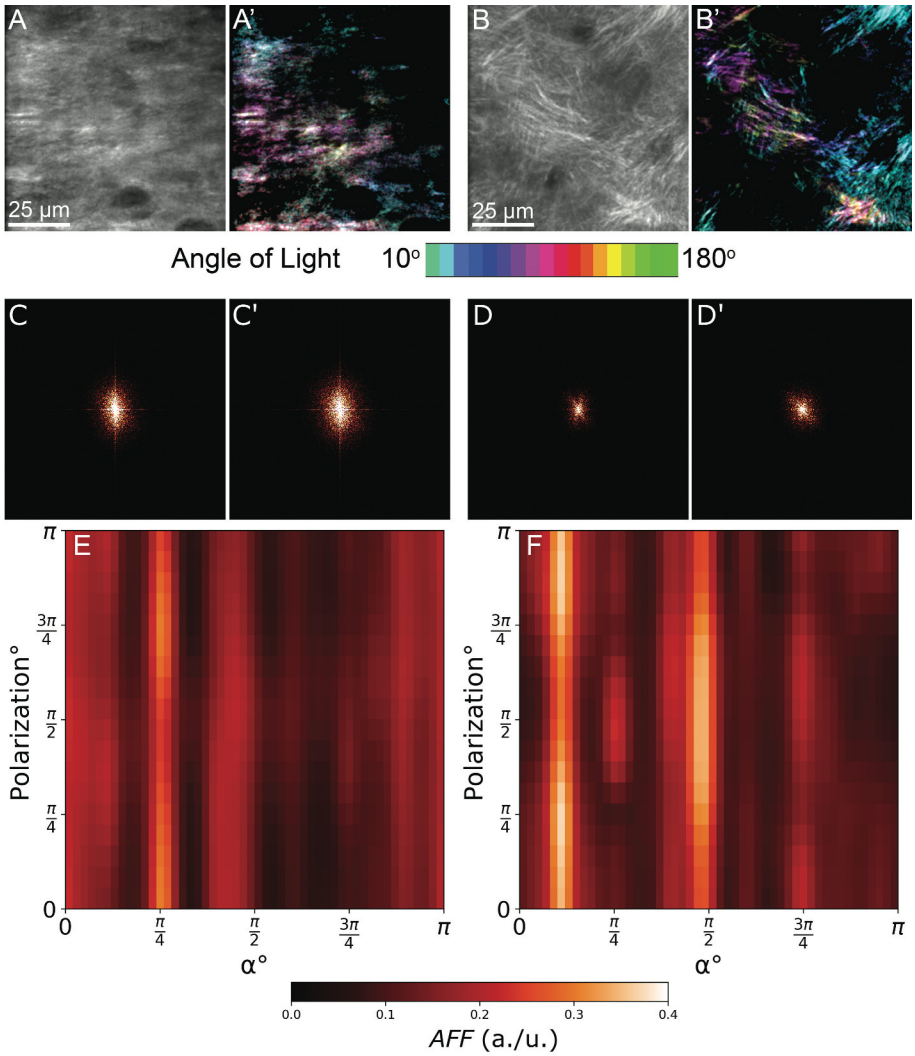

Figure 4. The angular Fourier filter (AFF) applied for the polarimetric analysis of bone collagen structures. Second harmonic generation data was recorded within one mean-free-path from the surface of juvenile (a), and an adult (b) mouse skull. (a′) and (b′) show a polarization-encoded presentation of the polarimetric data. A juvenile skull has a less compact structure due to the natural remodeling of the bone that occurs continuously. Therefore, the adult skull has a more developed and well-defined collagen structure. Fourier transforms of images, with 50° and 90° input light from juvenile dataset (a) are shown in (c) and (c′). Similarly, (d) and (d′) show Fourier transforms of 50° and 90° images from the adult dataset (b). The AFF histograms are shown in (e and f). (f) shows strong peaks that follow a sinusoidal trend with the input polarization.

structure beneath a layer of unorganized tissue (Figure 5(i)). Therefore, the RFF indicates an organized muscle fiber throughout the resolvable depth range, but not when tissue damage disrupts the structure.

The sample size for the experiments shown were n = 20 Z-stacks across different muscle and bone positions across 2 mice per condition; the techniques have been successfully applied to study the VML model in reference[37].

4. Conclusion

The metrics presented here provide methods for the analysis of tissue healthiness and regeneration for structures such as bone and muscle with periodic structural constructs. The use of Fourier-based metrics enables analysis of the frequency contents that can produce intensity-independent information[41,42]. The independence of this metric from the intensity reduces error that spatial domain analysis may encounter due to intensity fluctuations and different thresholding levels. For instance, if a fluorescent image has different shades in different regions, this metric will equally weight their measures. Our implementation of the AFF extracts angular information from the images and enables distinguishing structural difference between an intact muscle structure, a VML injured one, and during the healing process. AFF analysis of the osseous structures also exhibits features that were not readily visible between juvenile and adult skulls. The RFF metric complements the AFF metric by

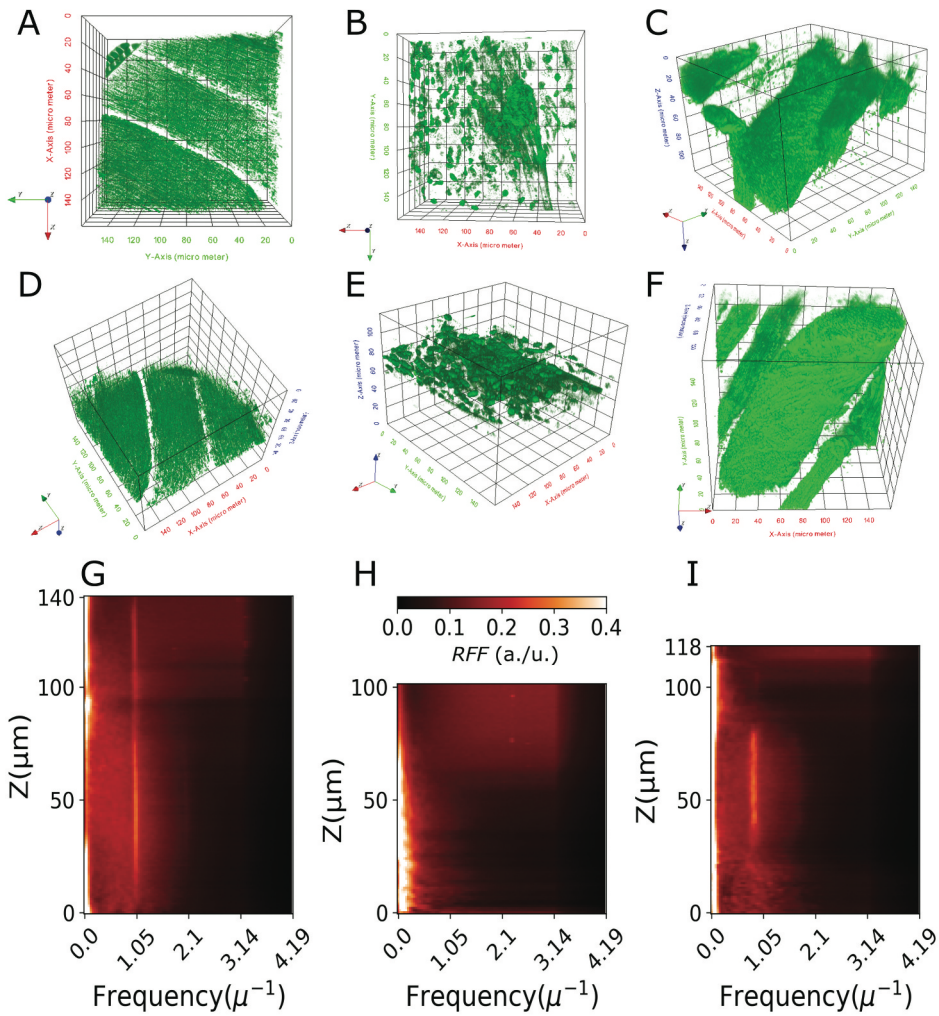

Figure 5. Radial Fourier Filtering (RFF), used for the description of TA muscle in intact (a), 7 days post-VML injury (b), and 30 days post-injury (c). A second 3D view of each sample (a-c) is shown in panels (d-f) for a better understanding of the structure. The RFF histograms are shown in panels (g-i). The intact muscle (g) shows a continuous peak at their characteristic frequency over the whole volume. In the 7 days post-VML injury sample, inflammatory cells are covering the muscle and due to lack of the muscle structure, no significant peak can be observed (h). By 30 days post-injury, the inflammatory cells are gone, but there is a disorganized fiber structure on top of an organized muscle; hence a peak is observed within the depth range that has the organized muscle (i).

extracting frequency information regardless of angularity. We implemented this metric on muscle structure and showed that it could produce a new dimension of data for analyzing a healing muscle with VML injury. In conclusion, the metrics provided here can be used by scientists in the field of musculoskeletal biology for analysis of the healthiness and regeneration of tissues. The toolsets provided in this research can also be applied to other label-free imaging methods such as auto-fluorescent imaging of NAD(H) and FAD for simultaneous structural and metabolism analysis.

Acknowledgments

Opinions, interpretations, conclusions and recommendations are those of the authors and are not necessarily endorsed by the Department of Defense.

Disclosure statement

The authors report no conflicts of interest.

Funding

This work was supported by the National Institutes of Health [R21EB027802]; National Science Foundation [1706916]; Georgia Tech Marcus Center; Georgia Partners in Medicine REM; U.S. Department of Defense [W81XWH-18-1-0710].

ORCID

Kayvan Forouhesh Tehrani http://orcid.org/0000-0002-3766-616X
Emily G. Pendleton http://orcid.org/0000-0002-2487-1009

W. Michael Southern http://orcid.org/0000-0001-8794-9064
Jarrod A. Call http://orcid.org/0000-0002-1094-4940
Luke J. Mortensen http://orcid.org/0000-0002-4331-4099

Data availability

The data that support the findings of this study are available from the corresponding author upon reasonable request.

References

1. Glancy B, Hartnell LM, Malide D, Yu Z-X, Combs CA, Connelly PS, Subramaniam S, Balaban RS. Mitochondrial reticulum for cellular energy distribution in muscle. Nature. 2015;523(7562):617–620. doi:10.1038/nature14614.
2. Mishra P, Varuzhanyan G, Pham AH, Chan DC. Mitochondrial dynamics is a distinguishing feature of skeletal muscle fiber types and regulates organellar compartmentalization. Cell Metab. 2015;22 (6):1033–1044.doi:10.1016/j.cmet.2015.09.027.
3. Tehrani KF, Pendleton EG, Southern WM, Call JA, Mortensen LJ.Two-photon deep-tissue spatially resolved mitochondrial imaging using membrane potential fluorescence fluctuations. Biomed Opt Express. 2018;9(1):254–259.doi:10.1364/BOE.9.000254.
4. Wang T, Zhang XP, Bikle DD.Osteogenic differentiation of periosteal cells during fracture healing. J Cell Physiol. 2017;232(5):913–921.doi:10.1002/jcp.25641.
5. Wang X, Bank RA, TeKoppele JM, Agrawal CM.The role of collagen in determining bone mechanical properties. J Orthopaed Res off Publ Orthopaed Res Soc. 2001;19(6):1021–1026.doi:10.1016/S0736-0266(01)00047-X.
6. Zimmermann EA, Schaible E, Bale H, Barth HD, Tang SY, Reichert P, Busse B, Alliston T, Ager JW 3rd, Ritchie RO.Age-related changes in the plasticity and toughness of human cortical bone at multiple length scales. Proc Natl Acad Sci U S A. 2011;108 (35):14416–14421.doi:10.1073/pnas.1107966108.
7. Mortensen LJ, Alt C, Turcotte R, Masek M, Liu T-M, Côté DC, Xu C, Intini G, Lin CP.Femtosecond laser bone ablation with a high repetition rate fiber laser source. Biomed Opt Express. 2015;6(1):32–42. doi:10.1364/BOE.6.000032.
8. Carpenter AE, Jones TR, Lamprecht MR, Clarke C, Kang IH, Friman O, Guertin DA, Chang JH, Lindquist RA, Moffat J, Golland P, Sabatini DM. CellProfiler: image analysis software for identifying and quantifying cell phenotypes. Genome Biol. 2006;7 (10):R100.doi:10.1186/gb-2006-7-10-r100.
9. Hartmann J, Wong M, Gallo E, Gilmour D. An image-based data-driven analysis of cellular architecture in a developing tissue. eLife. 2020;9:e55913.
10. Aeffner F, Zarella MD, Buchbinder N, Bui MM, Goodman MR, Hartman DJ, Lujan GM, Molani MA, Parwani AV, Lillard K, Turner OC, Vemuri VNP, Yuil-Valdes AG, Bowman D.Introduction to digital image analysis in whole-slide imaging: a white paper from the digital pathology association. J Pathol Inform. 2019;10 (1):9.doi:10.4103/jpi.jpi_82_18.
11. Bychkov D, Linder N, Turkki R, Nordling S, Kovanen PE, Verrill C, Walliander M, Lundin M, Haglund C, Lundin J.Deep learning based tissue analysis predicts outcome in colorectal cancer. Sci Rep. 2018;8(1):3395.doi:10.1038/s41598-018-21758-3.
12. Kuhl FP, Giardina CR.Elliptic Fourier features of a closed contour. Comput Graph Image Process. 1982;18 (3):236–258.doi:10.1016/0146-664X(82)90034-X.
13. Iwata H, Ukai Y, Computer Program SHAPE:A. Package for quantitative evaluation of biological shapes based on elliptic Fourier descriptors. J Heredity. 2002;93(5):384–385.doi:10.1093/jhered/93.5.384.
14. Campagnola PJ, Loew LM.Second-harmonic imaging microscopy for visualizing biomolecular arrays in cells, tissues and organisms. Nat Biotech. 2003;21 (11):1356–1360.doi:10.1038/nbt894.
15. Chaudhary R, Campbell KR, Tilbury KB, Vanderby R Jr., Block WF, Kijowski R, Campagnola PJ.Articular cartilage zonal differentiation via 3D Second-Harmonic Generation imaging microscopy. Connect Tissue Res. 2015;56(2):76–86.doi:10.3109/03008207.2015.1013192.
16. Mostaço-Guidolin LB, Ko AC, Wang F, Xiang B, Hewko M, Tian G, Major A, Shiomi M, Sowa MG. Collagen morphology and texture analysis: from statistics to classification. Sci Rep. 2013;3(1):2190. doi:10.1038/srep02190.
17. Ghazaryan A, Tsai H, Hayrapetyan G, Chen W-L, Chen Y-F, Jeong M-Y, Kim C-S, Chen S-J, Dong C-Y.Analysis of collagen fiber domain organization by Fourier second harmonic generation microscopy. J Biomed Opt. 2012;18(3):031105. doi:10.1117/1.JBO.18.3.031105.
18. Xylas J, Quinn KP, Hunter M, Georgakoudi I. Improved Fourier-based characterization of intracellular fractal features. Opt Express. 2012;20 (21):23442–23455.doi:10.1364/OE.20.023442.
19. Quinn KP, Sridharan GV, Hayden RS, Kaplan DL, Lee K, Georgakoudi I.Quantitative metabolic imaging using endogenous fluorescence to detect stem cell differentiation. Sci Rep. 2013;3(1):3432.doi:10.1038/srep03432.
20. Pouli D, Balu M, Alonzo CA, Liu Z, Quinn KP, Rius-Diaz F, Harris RM, Kelly KM, Tromberg BJ, Georgakoudi I. Imaging mitochondrial dynamics in human skin reveals depth-dependent hypoxia and malignant potential for diagnosis. Sci Transl Med. 2016;8(367):367ra169–367ra169.doi:10.1126/scitranslmed.aag2202.
21. Yildirim M, Quinn KP, Kobler JB, Zeitels SM, Georgakoudi I, Ben-Yakar A.Quantitative differentiation of normal and scarred tissues using second-harmonic generation microscopy. Scanning. 2016;38(6):684–693.doi:10.1002/sca.21316.
22. Mashiko D, Ikawa M, Fujimoto K. Mouse spermatozoa with higher fertilization rates have thinner nuclei. PeerJ. 2017;5:e3913.doi:10.7717/peerj.3913.
23. Plotnikov S, Juneja V, Isaacson AB, Mohler WA, Campagnola PJ.Optical clearing for improved contrast in second harmonic generation imaging of skeletal

muscle. Biophys J. 2006;90(1):328–339.doi:10.1529/biophysj.105.066944.
24. Zeitoune AA, Luna JS, Sanchez Salas K, Erbes L, Cesar CL, Andrade LA, Carvahlo HF, Bottcher-Luiz F, Casco VH, Adur J. Epithelial ovarian cancer diagnosis of second-harmonic generation images: a semiautomatic collagen fibers quantification protocol. Cancer Inform. 2017;16:1176935117690162. doi:10.1177/1176935117690162.
25. Hristu R, Stanciu SG, Tranca DE, Stanciu GA. Improved quantification of collagen anisotropy with polarization-resolved second harmonic generation microscopy. J Biophoton. 2017;10(9):1171–1179. doi:10.1002/jbio.201600197.
26. Lau TY, Ambekar R, Toussaint KC.Quantification of collagen fiber organization using three-dimensional Fourier transform-second-harmonic generation imaging. Opt Express. 2012;20(19):21821–21832. doi:10.1364/OE.20.021821.
27. Ambekar R, Chittenden M, Jasiuk I, Toussaint KC Jr. Quantitative second-harmonic generation microscopy for imaging porcine cortical bone: comparison to SEM and its potential to investigate age-related changes. Bone. 2012;50(3):643–650.doi:10.1016/j.bone.2011.11.013.
28. Fung DT, Sereysky JB, Basta-Pljakic J, Laudier DM, Huq R, Jepsen KJ, Schaffler MB, Flatow EL.Second harmonic generation imaging and Fourier transform spectral analysis reveal damage in fatigue-loaded tendons. Ann Biomed Eng. 2010;38(5):1741–1751. doi:10.1007/s10439-010-9976-7.
29. Wang M, Knoesen A.Rotation- and scale-invariant texture features based on spectral moment invariants. J Opt Soc Am A. 2007;24(9):2550–2557.doi:10.1364/JOSAA.24.002550.
30. Wang M, Reiser KM, Knoesen A.Spectral moment invariant analysis of disorder in polarization-modulated second-harmonic-generation images obtained from collagen assemblies. J Opt Soc Am A. 2007;24(11):3573–3586.doi:10.1364/JOSAA.24.003573.
31. Reiser K, Bratton C, Yankelevich D, Knoesen A, Rocha-Mendoza I, Lotz J.Quantitative analysis of structural disorder in intervertebral disks using second harmonic generation imaging: comparison with morphometric analysis. J Biomed Opt. 2007;12(6):064019.doi:10.1117/1.2812631.
32. Pijanka JK, Markov PP, Midgett D, Paterson NG, White N, Blain EJ, Nguyen TD, Quigley HA, Boote C.Quantification of collagen fiber structure using second harmonic generation imaging and two-dimensional discrete Fourier transform analysis: application to the human optic nerve head. J Biophoton. 2019;12(5):e201800376.doi:10.1002/jbio.201800376.
33. Reiser K, Stoller P, Knoesen A.Three-dimensional geometry of collagenous tissues by second harmonic polarimetry. Sci Rep. 2017;7(1):2642.doi:10.1038/s41598-017-02326-7.
34. Tehrani KF, Latchoumane CV, Southern WM, Pendleton EG, Maslesa A, Karumbaiah L, Call JA, Mortensen LJ.Five-dimensional two-photon volumetric microscopy of in-vivo dynamic activities using liquid lens remote focusing. Biomed Opt Express. 2019;10(7):3591–3604.doi:10.1364/BOE.10.003591.
35. Pham AH, McCaffery JM, Chan DC.Mouse lines with photo-activatable mitochondria to study mitochondrial dynamics. Genesis. 2012;50(11):833–843.doi:10.1002/dvg.22050.
36. Greising SM, Warren GL, Southern WM, Nichenko AS, Qualls AE, Corona BT, Call JA.Early rehabilitation for volumetric muscle loss injury augments endogenous regenerative aspects of muscle strength and oxidative capacity. BMC Musculoskelet Disord. 2018;19(1):173.doi:10.1186/s12891-018-2095-6.
37. Southern WM, Nichenko AS, Tehrani KF, McGranahan MJ, Krishnan L, Qualls AE, Jenkins NT, Mortensen LJ, Yin H, Yin A, Guldberg RE, Greising SM, Call JA.PGC-1α overexpression partially rescues impaired oxidative and contractile pathophysiology following volumetric muscle loss injury. Sci Rep. 2019;9(1):4079.doi:10.1038/s41598-019-40606-6.
38. Abbe E. A contribution to the theory of the microscope, and the nature of microscopic vision. Proc Bristol Nat Soc. 1874;1:200–272.
39. Chen X, Raggio C, Campagnola PJ.Second-harmonic generation circular dichroism studies of osteogenesis imperfecta. Opt Lett. 2012;37(18):3837–3839. doi:10.1364/OL.37.003837.
40. Tehrani KF, Kner P, Mortensen LJ.Characterization of wavefront errors in mouse cranial bone using second-harmonic generation. J Biomed Opt. 2017;22(3):036012.doi:10.1117/1.JBO.22.3.036012.
41. Tehrani KF, Xu J, Zhang Y, Shen P, Kner P.Adaptive optics stochastic optical reconstruction microscopy (AO-STORM) using a genetic algorithm. Opt Express. 2015;23(10):13677–13692.doi:10.1364/OE.23.013677.
42. Tehrani KF, Zhang Y, Shen P, Kner P.Adaptive optics stochastic optical reconstruction microscopy (AO-STORM) by particle swarm optimization. Biomed Opt Express. 2017;8(11):5087–5097. doi:10.1364/BOE.8.005087.